Correlation of the Molecular Electrostatic Potential Surface of an Enzymatic Transition State with Novel Transition-State Inhibitors†

Benjamin A. Horenstein and Vern L. Schramm*

Department of Biochemistry, Albert Einstein College of Medicine of Yeshiva University, 1300 Morris Park Avenue, Bronx, New York 10461

Received April 28, 1993; Revised Manuscript Received July 6, 1993•

ABSTRACT: The transition state stabilized by nucleoside hydrolase from *Crithidia fasciculata* is characterized by nearly complete glycosidic bond cleavage and oxycarbonium character in the ribosyl group [Horenstein, B. A., Parkin, D. W., Estupinan, B., & Schramm, V. L. (1991) *Biochemistry 30,* 10788–10795]. The electrostatic potential surface of the transition state provides detailed information which should be useful in the design of transition-state analogues [Horenstein, B. A., & Schramm, V. L. (1993) *Biochemistry 32,* 7089–7097]. The electrostatic potential surface of inosine at the transition state contains a distributed positive charge resulting from the oxycarbonium ion character of the ribosyl ring. The ribosyl ring pucker is 3′-exo as a result of the near sp^2 hybridization at C1′ of the ribose ring. A series of transition-state analogues have been synthesized which incorporate single or combined features of the transition state. Each feature of the transition state was analyzed for its contribution to binding energy. Kinetic inhibition constants correlate with the similarity of the inhibitor to the experimentally determined transition-state structure. Dissociation constants for the substrate and products of the reaction of inosine, hypoxanthine, and ribose are 380, 6200, and 700 μM, respectively. A transition-state analogue was synthesized which contains the required hydroxyl groups of the ribose ring, the positive charge feature of the oxycarbonium ion, and a hydrophobic mimic of the purine ring. The inhibitor 1(*S*)-phenyl-1,4-dideoxy-1,4-iminoribitol acts as a competitive inhibitor with respect to inosine with a dissociation constant of 0.17 μM. In addition, the inhibitor exhibits slow-onset inhibition which provides a final equilibrium dissociation constant of approximately 0.03 μM. The affinity of inhibitor binding correlates to the match between the electrostatic potential surfaces of the inhibitors and the transition states but less well to the geometric similarity. The results establish that an enzymatic transition state characterized by a family of kinetic isotope effects, bond vibrational analysis, and molecular electrostatic potentials facilitates the design of transition-state inhibitors.

Inhibitors which contain structural features of the transition states of enzymatic reactions are exceptionally powerful inhibitors (Wolfenden, 1972; Lienhard, 1973). Many of the known inhibitors that qualify as transition-state analogues were discovered as natural products, such as the protease inhibitor pepstatin, the adenosine deaminase inhibitor (*R*)-deoxycoformycin, glycosidase inhibitors such as nojirimycin, and the hydroxymethylglutaryl-coenzyme A reductase inhibitor compactin (Umezawa et al., 1970; Sawa et al., 1967; Niwa et al., 1970; Endo et al., 1976). A goal of enzymatic transition-state analysis has been to characterize the transition-state structure of an enzymatic reaction with sufficient accuracy to permit the logical design of transition-state inhibitors. In this work, transition-state structure is applied in a new approach to the evaluation and design of transition-state analogue inhibitors. The method is specifically applied to nucleoside hydrolase, a purine salvage enzyme from the trypanosome *Crithidia fasciculata.*

The approach employs transition-state analysis of an enzymatic reaction to describe the geometry and electrostatic features of the transition state. This information is derived from multiple, experimentally determined kinetic isotope effects which report on transition-state structure (Horenstein et al., 1991). The resulting geometry is characterized in terms of its molecular electrostatic potential (MEP),[1] displayed on a van der Waals surface, providing a template for inhibitor design (Horenstein & Schramm, 1993). Molecular electrostatic potentials have been used previously to analyze enzyme inhibitors. For example, binding interactions of trypsin and bovine plasma trypsin inhibitor have been described in terms of complementary MEP (Weiner et al., 1982), and binding constants have been correlated with MEP in a series of inhibitors (Thomson, 1989). The present study extends previous work by proposing the transition-state MEP as a de novo design tool. The MEP of an experimentally determined transition state is used as a predictive model to propose inhibitors with similar MEP as geometric and electronic mimics of the transition state.

The experimentally determined transition-state structure for inosine in the nucleoside hydrolase reaction is shown in Figure 1. The molecular electrostatic potential for the structure in Figure 1 is superimposed on a van der Waals surface with the attacking nucleophile water present and is shown in the upper panel of Figure 2. The molecular electrostatic potential surface for the transition-state structure without the attacking water nucleophile is shown in the lower panel of Figure 2. Note the positive charge on the ribosyl ring in Figure 2. In the inhibitor design, attempts have been made to mimic both the geometry and the charge of the structure

† This work was supported by Research Grants GM41916 and GM21083 from the NIH and Fellowship PF3298 from the American Cancer Society. The authors gratefully acknowledge a computational grant from the Pittsburgh Supercomputer Center.

• Abstract published in *Advance ACS Abstracts,* September 1, 1993.

[1] Abbreviations: MEP, molecular electrostatic potential; anhydroribitol, 1,4-anhydro-D-ribitol; iminoribitol, 1,4-dideoxy-1,4-iminoribitol; imidazolyliminoribitol, 1(*S*)-(4-imidazolyl)-1,4-dideoxy-1,4-iminoribitol; phenyliminoribitol, 1(*S*)-phenyl-1,4-dideoxy-1,4-iminoribitol.

0006-2960/93/0432-9917$04.00/0

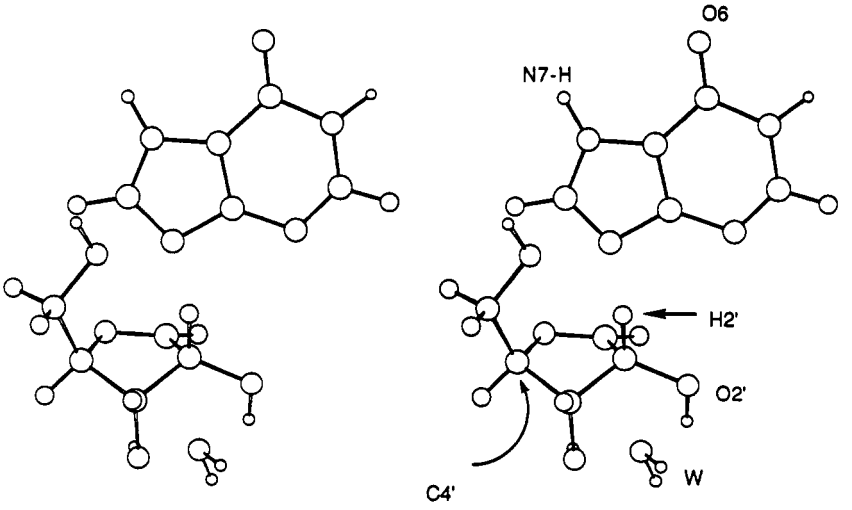

FIGURE 1: Stereo diagram of the transition-state structure for nucleoside hydrolase. The geometric arrangement and atom numbering are indicated for inosine at the transition state of nucleoside hydrolase. Differences from inosine include protonation of the leaving group at N7, a C1′–N9 bond length of 1.98 Å compared to a bond length of 1.48 Å for the reactant, a C1′–O′H distance of 3.0 Å for the attacking oxygen (water) nucleophile, rehybridization of C1′ to near sp^2 geometry, altered ribose ring pucker to the 3′-exo configuration, compared to the 3′-endo configuration for the reactant inosine, and altered conformation and distortion of the C5′ hydroxymethyl group to position it above the ribose ring (Horenstein et al., 1991; Horenstein & Schramm, 1993).

in Figure 2 (lower panel). At the transition state, the attacking water is an enzyme-bound nucleophile which will be provided by the enzyme (Parkin et al., 1991a). The key features of the transition state include the development of a partially dispersed positive charge originating from electron departure from the glycosidic bond, a 3′-exo ribosyl conformation, and the hydrophobic, N7 protonated hypoxanthine as the leaving group. The features of this structure provide the blueprint for design of transition-state analogues.

MATERIALS AND METHODS

Transition-State Modeling. The experimental approach for determination of the transition-state structure of nucleoside hydrolase was reported previously (Horenstein et al., 1991; Horenstein & Schramm, 1993). Briefly, the geometry of the model was obtained by vibrational analysis of experimental kinetic isotope effects using the BEBOVIB-IV program (Sims et al., 1977; Sims & Lewis, 1984). The molecular electrostatic potential of the transition state was calculated using the CUBE = DENSITY and CUBE = POTENTIAL functions in Gaussian92 self-consistent-field calculations (Frisch et al., 1992). The results were graphically displayed using the AVS Chemistry Viewer programs (Advanced Visual Systems Inc. and Molecular Simulations Inc.).

Inhibitor Modeling. The goal of the inhibitor modeling was to compare candidate inhibitors to the transition-state model in terms of geometry and charge properties. All inhibitors examined contained a five-membered ring with hydroxyls to resemble a ribosyl residue. The ribosyl ring mimic was placed in a 3′-exo ring conformation analogous to the transition state of inosine stabilized by nucleoside hydrolase. Similarly, hydroxyl group rotamers at O5′, O3′, and O2′ were fixed at values analogous to those of the transition state. The rationale for these choices was that interconversion of various ring conformations of the ribofuranosyl residue is accomplished with relatively small energetic barriers. Ribosyl residue conformations analogous to that of the transition state will be enforced upon binding to the active site of nucleoside hydrolase. Each inhibitor in the 3′-exo ring conformation was minimized in bond length coordinates with Gaussian92 using the STO-3G basis set. This minimization serves to "relax" bonds within the context of the basis set, minimizing artifactual contributions to the electrostatic potential due to nonequilibrium bond lengths. The STO-3G basis set provided a description of the molecular electrostatic potential which was qualitatively identical to that calculated with the 6-31G basis set[2] (Horenstein & Schramm, 1993). An ab initio method was employed in preference to semiempirical techniques to avoid uncertainties relating to parametrization.

Nucleoside Hydrolase. Nucleoside hydrolase was purified from *C. fasciculata* as described by Parkin et al. (1991a). The enzyme was >95% homogeneous as judged by denaturing polyacrylamide gel electrophoresis.

Inhibitors. The structures of substrates, products, and transition-state analogues employed in this study are shown in Figure 3. Inosine (**1**), ribose (**2**), and hypoxanthine (**3**) were purchased from Sigma. 1,4-Anhydro-D-ribitol (**4**) was synthesized by the method of Bennek and Gray (1987) and the structure confirmed by X-ray crystallography. Ribonolactone (**5**) (Sigma) was recrystallized from 80% aqueous ethanol before use. 1,4-Deoxy-1,4-iminoribitol (**6**) was synthesized by the method of Fleet and Son (1988). 1(*S*)-(4-Imidazolyl)-1,4-dideoxy-1,4-iminoribitol (**7**) was synthesized by a route analogous to that used for the phenylpyrrolidine described below. The imidazoyl residue was added to the pyrroline as its 4-lithio-2-thiophenyl-N^3-[[2-(trimethylsilyl)ethoxy]methyl] derivative. The protected product was deblocked by removal of the thiophenyl ether with Raney nickel, followed by acidic hydrolysis. 1(*S*)-Phenyl-1,4-dideoxy-1,4-iminoribitol (**8**) was synthesized from the 5-(*tert*-butyldimethylsilyl)-2,3-isopropylidene ketal derivative of **6**. The protected **6** was N-chlorinated with *N*-chlorosuccinimide in pentane, followed by dehydrohalogenation with lithium tetramethylpiperidide in tetrahydrofuran at −78 °C. The resulting 1-pyrroline was reacted with phenylmagnesium bromide to provide the protected inhibitor. The stereo- and regiochemistry of the protected product was established by

[2] The *absolute value* of the MEP was sensitive to the basis set. However, the MEP information is used to compare *relative* differences between the transition state and inhibitors. Thus, the absolute value of the MEP is not crucial for matching inhibitor to transition MEP as long as the same basis is used for both.

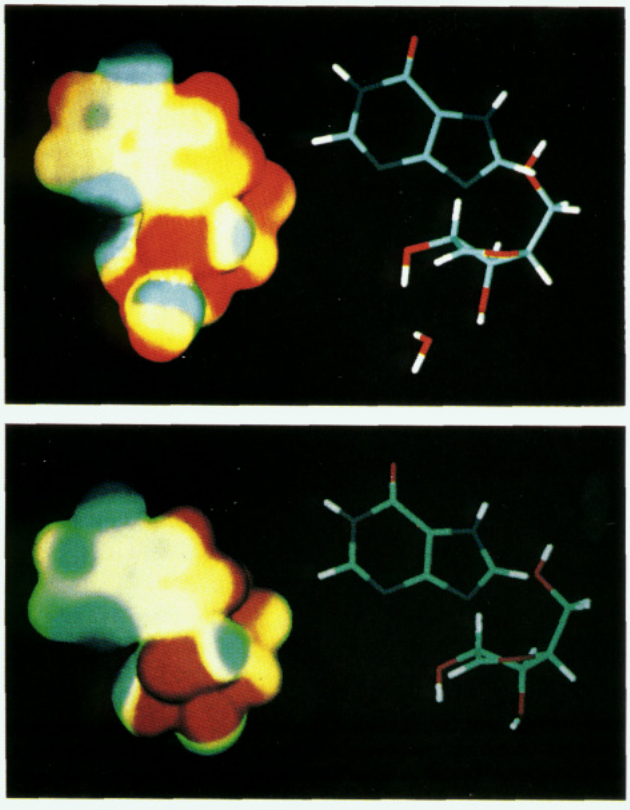

FIGURE 2: Molecular electrostatic potential surfaces for the transition state of nucleoside hydrolase. In the upper panel, the molecular electrostatic potential of the structure in Figure 1 is shown together with the stick model in the same orientation. In the lower panel, the molecular electrostatic potential surface is shown for the transition state *without* the preassociated water nucleophile. The orientation is the same in Figure 1 and both panels shown above. The stick models in both panels use the colors red = oxygen, blue = nitrogen, green = carbon, and white = hydrogen. The molecular electrostatic potential surface uses blue to represent negative electrostatic potential and red to represent positive electrostatic potential, with green and yellow being less negative/positive than blue and red, respectively. The red regions which do not correspond to OH or NH groups represent positive electrostatic potential arising from the oxycarbonium ion. The experiments leading to these structures are described in Horenstein et al. (1991) and Horenstein and Schramm (1993).

difference nuclear Overhauser effect experiments. Removal of the *tert*-butyldimethylsilyl and isopropylidene ketal protecting groups was achieved by hydrolysis in 50% aqueous trifluoroacetic acid. The product was purified on Dowex 50×8 (H^+ form) resin. The purified material showed NMR, mass spectrometry, and high-resolution mass spectra consistent with the desired product. A detailed description of the synthesis and chemical characterization of these compounds is in preparation.

Determination of Inhibition Constants. Inhibition studies of nucleoside hydrolase were performed with inosine as the substrate at 30 °C. Initial reaction rates were determined by spectrophotometric assay, monitoring the decrease in absorption at 280 nm upon conversion of inosine to hypoxanthine and ribose. Reactions were initiated by addition of enzyme to a 1.0-mL reaction mixture in a 1-cm cuvette. Rates were measured at five concentrations of inosine and at least three different concentrations of inhibitor. Data were fit to the equations for competitive and noncompetitive inhibition using the kinetic programs of Cleland (1977). The inhibition constants obtained from these fits together with buffer and pH conditions are summarized in the text. Inhibition constants for additional compounds described in the text were obtained from Parkin et al. (1991a).

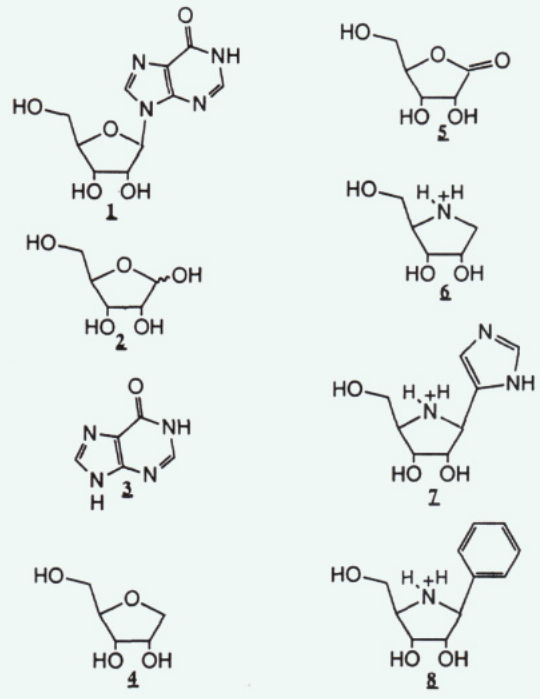

FIGURE 3: Substrate, product, and inhibitors for nucleoside hydrolase. The substrate inosine (**1**) and products ribose (**2**) and hypoxanthine (**3**) are compared to analogues with various features of the transition state. 1,4-Anhydro-D-ribitol (**4**) permits analysis of the contribution of binding by the 1-hydroxy of ribose. Ribonolactone (**5**) contains an sp^2-hybridized carbon at C1, causing the ring pucker to adopt the 3′-exo configuration, similar to the 3′-exo configuration of the transition state (cf Figure 1). A charged analogue of the ribosyl transition-state structure is 1,4-dideoxy-1,4-iminoribitol (**6**), which resembles the charge developed on ribose in the transition state. An analogue which contains a proton acceptor as the aglycon is 1(*S*)-(4-imidazolyl)-1,4-dideoxy-1,4-iminoribitol (**7**), which also incorporates the positive charge feature of the oxycarbonium ion. The hydrophobic nature of the aglycon and the positive charge of the oxycarbonium ion are incorporated into 1(*S*)-phenyl-1,4-dideoxy-1,4-iminoribitol (**8**).

RESULTS

Electrostatic Properties of Substrate, Product, and Inhibitors of Nucleoside Hydrolase. Structural formulas and molecular electrostatic potential surfaces with the corresponding stick figures for inosine (**1**), ribose (**2**), hypoxanthine (**3**), 1,4-anhydro-D-ribitol (**4**), ribonolactone (**5**), 1,4-dideoxy-1,4-iminoribitol (**6**), 1(*S*)-(4-imidazolyl)-1,4-dideoxy-1,4-iminoribitol (**7**), and 1(*S*)-phenyl-1,4-dideoxy-1,4-iminoribitol (**8**) are shown in Figures 3 and 4, respectively. For all of the compounds containing the ribosyl residue or its analogues, the electrostatic potentials about the hydroxyls are similar. The oxygens exhibit equivalent negative electrostatic potential, while hydrogens attached to oxygen are positive in electrostatic potential, identifying these sites as hydrogen bond acceptor and donor sites, respectively. The molecular electrostatic potential surfaces for inosine and ribose differ substantially from that for the transition-state surface (compare Figure 4A,B with Figure 2). The transition state contains greater positive electron potential residing in the region of C1′–O4′, relative to the analogous position at C1′–O4′ of ribose. Ribonolactone (**5**) (panel D of Figure 4) is planar at C1, analogous to the planarity at C1′ of the transition state, and is known to have a crystal structure with 3′-exo ribosyl ring pucker (Kinoshita et al., 1981). Relative to ribose and the transition state, ribonolactone has a negative MEP corresponding to the lactone oxygens. It also differs sterically from the transition state by having an exocyclic carbonyl oxygen.

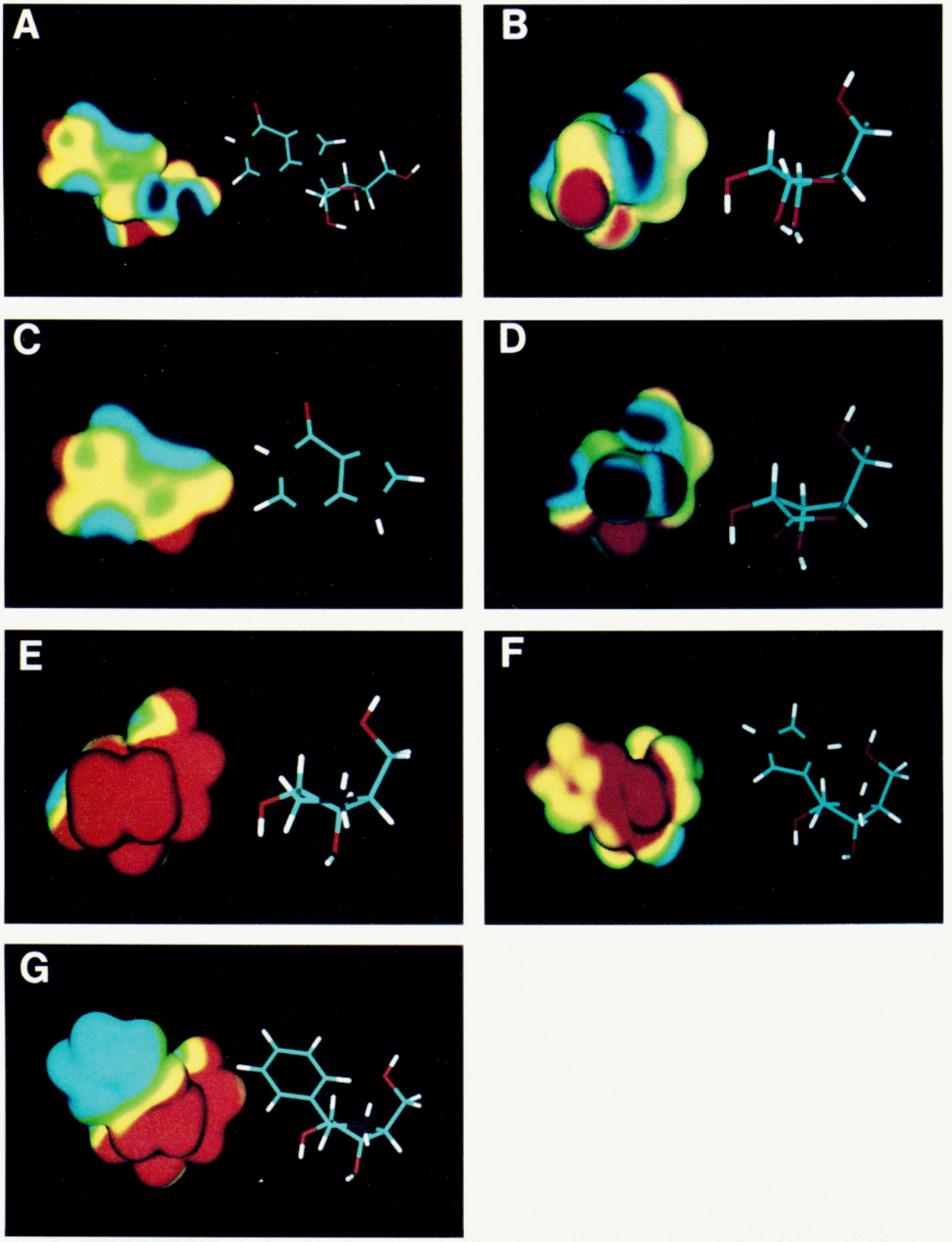

FIGURE 4: Molecular electrostatic potential surfaces for substrate, products, and inhibitors of nucleoside hydrolase. The structures and corresponding molecular electrostatic potential surfaces are shown together in each panel. The assignment of electrostatic potential is the same as described in the legend to Figure 1. The structure and molecular electrostatic potentials are shown for (A) inosine (**1**), (B) ribose (**2**), (C) hypoxanthine (**3**), (D) ribonolactone (**5**), (E) 1,4-dideoxy-1,4-iminoribitol (**6**), (F) 1(*S*)-(4-imidazolyl)-1,4-dideoxy-1,4-iminoribitol (**7**), and (G) 1(*S*)-phenyl-1,4-dideoxy-1,4-iminoribitol (**8**).

The effect of the 1-hydroxyl group was determined by inhibition studies with 1,4-anhydro-D-ribitol (**4**) which lacks the hydroxyl at C1. The absence of significant inhibition at 20 mM suggests that in the absence of ring charge (as found in **6**) the 1-hydroxyl is important for binding. Neither ribose (**2**) nor 1,4-anhydro-D-ribitol are good inhibitors.

Table I: Dissociation Constants for Compounds 1–8[a]

inhibitor	K_i (or K_m) (μM)
inosine (1)	380 ± 30
ribose (2)	700 ± 100
hypoxanthine (3)	6200 ± 900
1,4-anhydro-D-ribitol (4)	>10000
ribonolactone (5)	90 ± 20
1,4-dideoxy-1,4-iminoribitol (6)	4.5 ± 0.4
1(*S*)-(4-imidazolyl)-1,4-dideoxy-1,4-iminoribitol (7)	2.5 ± 0.2
1(*S*)-phenyl-1,4-dideoxy-1,4-iminoribitol (8)	0.17 ± 0.01 (0.03)[b]

[a] Data for compounds 1–3 were taken from Parkin et al. (1991). Kinetic analysis for 4–6 was in 50 mM mixed buffer containing equal concentrations of Mes–Mops–GlyGly–Gly, pH 7.5. Analysis of 7 and 8 was in 50 mM mixed buffer containing 50 mM Mes–BisTris, pH 7.5. All assays were at 30 °C. The inhibition constants are sensitive to buffer content (compare Tables I and III). [b] Estimated dissociation constant following the slow-onset inhibition.

A charge mimic of the oxycarbonium ion-like ribosyl group of the transition state is 1,4-dideoxy-1,4 iminoribitol (6) (panel E of Figure 4). The ammonium group between C1 and C4 confers a strongly positive MEP which mimics the charge present on ribose in the transition state. The imidazole analogue of the transition state (7) also mimics the oxycarbonium ion charge buildup via the ring ammonium ion and incorporates a protonation site in the imidazole ring, analogous to the protonation site for the transition state, at N7 of the hypoxanthine ring and is shown in its diprotic form (panel F of Figure 4). Note the positive electrostatic potential associated with N3 of the imidazole ring due to protonation. Comparison of the geometry of the imidazole inhibitor (7) with that of the transition state indicates that the imidazole ring resides midway between the region occupied by the pyrimidine and the imidazole rings of the hypoxanthine. Phenyliminoribitol (8) combines the positive charge of the ribosyl ring of the transition state with a hydrophobic group, which is linked via a C-glycosidic linkage. The MEP is positive in the region of the ammonium group, while the phenyl group is hydrophobic, producing a uniform slightly negative MEP over the phenyl ring (panel G of Figure 4). Comparison of the geometry of phenyliminoribitol to the transition state indicates that the phenyl ring resides in a region between that occupied by the pyrimidine and imidazolyl portions of the hypoxanthine ring in the transition state.

Kinetic Constants for Substrates, Products, and Inhibitors of Nucleoside Hydrolase. The kinetic and inhibition constants for inosine, products, and the transition state mimics are reported in Table I. The reaction products ribose and hypoxanthine are poor inhibitors, both binding less tightly than substrate inosine. Successive incorporation of transition-state features into the structure of the inhibitor results in decrease of the oberved K_i's. Ribonolactone (5) is a geometric transition-state mimic and binds 7.8 times tighter than product ribose and four times better than the substrate inosine. The charge mimic iminoribitol (6) binds nine times tighter than ribonolactone, suggesting the importance of charge recognition over geometric considerations. The imidazolyl iminoribitol (7) binds with an observed K_i of 2.5 μM, about 1.8 times tighter than the unsubstituted pyrrolidine, indicating that this proton-accepting aglycon undergoes favorable binding interactions with the enzyme. The phenyliminoribitol (8) binds to nucleoside hydrolase as a competitive inhibitor with an observed K_i of 0.17 μM, 2200 times tighter than does inosine. This result indicates that the hydrophobic phenyl ring makes a substantial contribution to the binding.

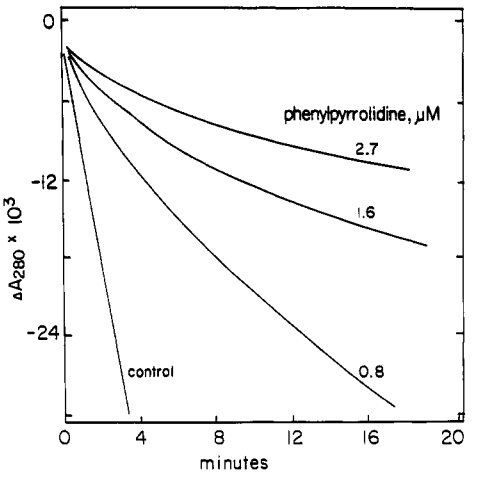

FIGURE 5: Slow-onset inhibition by 1(*S*)-phenyl-1,4-dideoxy-1,4-iminoribitol (phenyliminoribitol). The reactions were initiated by the addition of nucleoside hydrolase to reaction mixtures containing 50 mM triethanolamine, pH 7.5, 300 μM inosine, and the indicated concentrations of phenyliminoribitol. The decrease in absorbance at 280 nM was measured at 30 °C. The final enzyme concentration was 3.2×10^{-9} M. Mixing artifacts and the first 15–20 s of the reaction are not shown. The curve marked control contained no phenyliminoribitol.

Table II: Kinetic Constants for Substrates and Inhibitors of Nucleoside Hydrolase[a]

substrate/inhibitor	V_{max} (μmol min^{-1} mg^{-1})	K_m or $K_{i(app)}$[b] (μM)
inosine	50 ± 2	380 ± 30
adenosine	7.6 ± 0.2	460 ± 30
guanosine	2.70 ± 0.04[c]	420 ± 10
purine riboside	0.04 ± 0.01	145 ± 23
2′-deoxyadenosine	<0.0006	3200 ± 800[b]
3′-deoxyadenosine	<0.16	7290 ± 1100[b]
5′-deoxyadenosine	~0.008	11700 ± 500[b]
5′-deoxyinosine	~0.015	
7-deazaadenosine	<0.0008	2300 ± 400[b]
formycin B		1960 ± 410[b,d]

[a] Data are reproduced from Parkin et al. (1991). [b] $K_{i(app)}$ is an apparent inhibition constant determined at a single inosine concentration near the K_m value and three inhibitor concentrations, as described in Parkin et al. (1991). [c] This value was erroneously reported as 70 ± 0.04 in Parkin et al. (1991). [d] Formycin B is a C-glycoside and cannot act as a substrate.

Slow-Onset Inhibition by Phenyliminoribitol. The initial rate kinetics with phenyliminoribitol (8) as inhibitor gave linear competitive inhibition with a K_i of 0.17 μM (Table I). Initial rates are followed by a period of increased inhibition as indicated in Figure 5. The overall inhibition constant following slow-onset inhibition can be estimated to be approximately 30 nM on the basis of the initial and final rates of product formation in Figure 5. Incubation of enzyme with relatively high concentrations of phenyliminoribitol for extended time periods did not cause irreversible inhibition. Thus, the slow-onset inhibition is not due to covalent modification of the enzyme.

Ionization Constants for Iminoribitol Inhibitors. The pK_a values for iminoribitol (6) imidazolyliminoribitol (7), and phenyliminoribitol (8) were determined by titrating the acidic forms of the inhibitors with NaOH. The results provided pK_a values of 8.3 and 6.5, respectively, for 6 and 8. Imidazolyliminoribitol (7) gave pK_a values of 5.2 and 8.7. NMR analysis of 7 as a function of pH indicated that the imidazole group ionizes with the pK_a of 5.2 and the iminoribitol with the pK of 8.7. The effect of pH on inhibitor binding was estimated by measuring the inhibition constants at pH values from 6.0 to 8.5 (Table III).

Table III: Effect of pH on Inhibition Constants for Nucleoside Hydrolase[a]

	K_i values (μM) for		
pH	1,4-dideoxy-1,4-iminorbitol, pK_a 8.3	1(*S*)-(4-imidazolyl)-1,4-dideoxy-1,4-iminorbitol, pK_{a1} 5.2, pK_{a2} 8.7	1(*S*)-phenyl-1,4-dideoxy-1,4-iminoribitol, pK_a 6.5
6.0	71 ± 8	3.8 ± 0.3	0.33 ± 0.02
7.0	21 ± 4	2.5 ± 0.2	0.17 ± 0.01
8.5	5 ± 0.5	13 ± 3	1.22 ± 0.04

[a] Inhibition constants were determined by full kinetic analysis at 30 °C. Buffers were 50 mM mixed Mes–Bis Tris, titrated to the desired pH with HCl. For imidazolyliminoribitol pK_{a1} is for the imidazole ring and pK_{a2} is for the iminoribitol ring.

pH Dependence of Inhibition by Iminoribitol Inhibitors. Inhibition of nucleoside hydrolase by iminoribitol (**6**) is greatest at pH 8.5 and decreases 14-fold as the pH is decreased to 6.0. 1-Substituted iminoribitols show a different pattern with the highest affinity near pH 7.0 and decreasing affinity as pH varies above and below neutrality. The binding of inosine to nucleoside hydrolase is pH independent while V_{max} depends on two ionized groups with the pK_a near 6.1 (Parkin et al., 1991a). The observed inhibition patterns indicate that the iminoribitol inhibitors differ from substrate interactions with nucleoside hydrolase in that ionizable groups on both the enzyme and the inhibitors influence binding affinity. 1-Substitutions on the iminoribitol inhibitors cause additional changes in the properties of the enzyme–inhibitor interactions.

DISCUSSION

Features Required for Binding and Catalysis by Nucleoside Hydrolase. The observed Michaelis constant for the substrate inosine and observed K_i's for products ribose and hypoxanthine represent dissociation constants, since the mechanism for the enzyme has been shown to be rapid equilibrium and random with respect to dissociation of products (Parkin et al., 1991a). The dissociation constants for substrate and products can be compared to the K_i's for inhibitors to correlate structural contributions to binding energies. An important component for substrate recognition and catalysis is the ribose hydroxylation pattern. All three ribosyl hydroxyls were previously documented as required features for binding and catalysis, as evidenced by poor binding and low or absent catalytic activity associated with deoxynucleoside substrates (Parkin et al., 1991; Table II). In addition, a proton acceptor is required as part of the aglycon, since 7-deazaadenosine is not a substrate and is poorly bound. At 30 °C, the relative binding contributions of the 2′-, 3′-, and 5′-hydroxyls and N7 of the purine ring can be estimated to be −1.2, −1.7, −2.0, and −1.0 kcal/mol, respectively. The three ribosyl hydroxyl groups and N7 together contribute an observed −5.8 kcal/mol of substrate binding energy. On the basis of a dissociation constant of 380 μM, inosine binds to nucleoside hydrolase with a net binding energy of −4.7 kcal/mol; thus hydroxyl and N7 recognition alone provides sufficient energy for the observed binding. Energy from additional contacts with the O4′ oxygen, ribosyl hydrogens, and hydrophobic interactions with the hypoxanthine ring can provide energy in addition to that from the hydroxyls to contribute toward formation of the transition-state configuration.

Since the hydroxyls are required for binding and catalysis, their presence can be considered as elements of ground-state *and* transition-state recognition (Wolfenden & Kati, 1991). The observation of a remote ^{3}H secondary kinetic isotope effect at C5′ of inosine (Horenstein et al., 1991) is consistent with transition-state hydroxyl group binding, with some of the intrinsic binding energy being employed for catalysis. The upper limits for the ability of deoxynucleosides and analogues to function as substrates for nucleoside hydrolase are summarized in Table II. For example, 5′-deoxyinosine is at least 3×10^{-4} slower than inosine. This difference in rate corresponds to a minimum of 4.9 kcal/mol energy penalty in transition-state binding recognition which is lost on removal of the 5′-hydroxyl. The lower limits for transition-state recognition for the 3′- and 2′-hydroxyls and N7 can similarly be estimated to be >1.1, 2.5, and 3.2 kcal/mol. The sum of these contributions is a minimum of 11.7 kcal/mol. Since nucleoside hydrolase lowers the energy of activation by 17.8 kcal/mol relative to solvent catalysis (see below), only 6.1 kcal/mol additional binding energy is required to reach the transition state.

These observations indicate that the ribose hydroxylation pattern is required for the initial binding of substrates as well as for providing access to transition-state recognition elements from other features of substrate molecules. The energetic requirements for all ribose hydroxyls for both binding and catalysis establish the importance of incorporating the ribose hydroxylation pattern into a transition-state inhibitor. Since hydroxyls cause a distinct electrostatic potential pattern for hydrogen bond formation, their geometry is a crucial factor in electrostatic recognition.

Geometric Features of the Transition State. Transition-state analysis indicates that the ribosyl ring has a 3′-exo conformation at the transition state [Figure 1; see also Horenstein et al. (1991)]. In calculating the molecular electrostatic potential surfaces for inhibitors, the ribosyl ring geometry was taken to be 3′-exo. Facile interconversion of ring conformers occurs in the ribofuranosides (Angelotti et al., 1987), and it is assumed that the active site directs similar ring conformations for ribosyl- or iminoribitol-based inhibitors which mimic the transition state.

Ribonolactone provides a geometric model of the transition-state ribosyl group, since the planar geometry at C1 mimics the planar geometry of the oxycarbonium ion-like transition state. In addition, the X-ray crystal structure and solution conformation of ribonolactone establishes that it, like the transition state, has the 3′-exo conformation (Munns & Tollin, 1970; Angelotti et al., 1987). The K_i of 90 μM for ribonolactone compared to the K_m of 380 μM for inosine indicates a −0.9 kcal/mol energetic preference for binding. A portion of the additional binding energy may be ascribed to the contribution that planarity at C1 and the 3′-exo configuration makes toward transition-state recognition. However, on the basis of the results with anhydroribitol, the lactone oxygen also makes a contribution to binding. No significant binding of anhydroribitol (**4**) was detected at millimolar concentrations. The crystal structure of **4** indicates that it is 3′-endo in ring pucker, and molecular mechanics calculations indicate that the 3′-exo configuration is unfavorable by approximately 1 kcal/mol. However, ribonolactone binds more favorably by at least 2.8 kcal/mol. Thus both ribosyl ring geometry and the ability of the enzyme to interact with the oxygen at C1 are likely to be important for the binding of ribonolactone.

As additional geometric features of the transition-state structure are incorporated into the inhibitor, decreasing K_i values are observed. For example, the observation that the imidazolyliminoribitol (**7**) inhibits only 2-fold better than imininibitol (**6**) indicates that imidazole, as a mimic of the

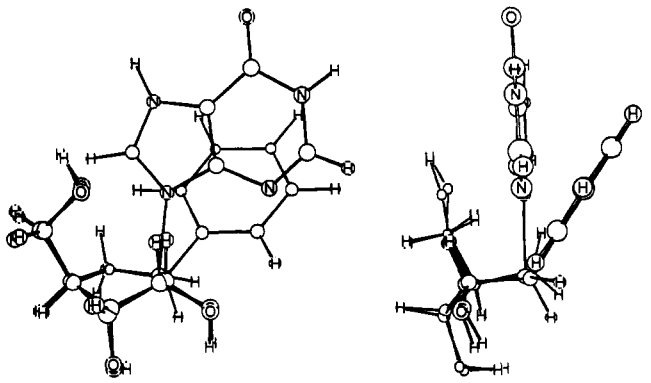

FIGURE 6: Comparison of aglycon positioning for the transition state of nucleoside hydrolase and a transition-state analogue inhibitor. The superimposed structures (left and right) place the ribosyl of the transition state and the iminoribitol of a transition-state inhibitor in isosteric conformations. The glycosyl torsion angle for the inhibitor phenyl ring is shown with the same torsion angle used for the hypoxanthine ring in the transition state (Figure 1). Bond lengths and angles of the transition-state structure are as described previously (Horenstein & Schramm, 1993). The left and right panels compare front and side views, respectively, of the transition-state aglycons using 1(*S*)-phenyl-1,4-dideoxy-1,4-iminoribitol (**8**) as the example of inhibitor alignment.

proton-accepting leaving group at the transition state, contributes only a small amount of favorable binding energy. The phenylpyrrolidine is a better inhibitor of nucleoside hydrolase, which indicates that the hydrophobic group provides more binding energy than does the imidazole group.

The C-glycosidic inhibitors have geometric differences compared to the transition-state structure (Figure 1A). In particular, the sp^3 hybridization at C1 of the inhibitors tilts the aglycon functionality away from the ribosyl residue. In the transition state, the trigonal planar geometry at C1′ places the departing aglycon–C1′ bond at approximately 90° from the plane defining the oxycarbonium ion. The result of this difference is that the aglycon of the inhibitors resides in the position midway between the pyrimidine and imidazolyl portions of hypoxanthine in the transition state but displaced in relation to ribose (Figure 6). Effective inhibition by the phenyliminoribitol but less so with the imidazolyliminoribitol indicates that the phenyl group binds via a favorable hydrophobic interaction, which the imidazole residue disfavors. The role of the imidazole as a proton acceptor mimic of the transition state is disfavored because it resides in the hydrophobic pocket midway between the pyrimidine and imidazolyl portions of hypoxanthine and is placed incorrectly to interact with the group which protonates N7 in the transition state (Figure 6). The positive MEP of N3 protonated **7** is not ideally placed to mimic the positive MEP around N7–C8 of hypoxanthine in the transition state (compare Figures 2 and 4F). An ideal isostere for the transition-state model would have a trigonal bipyrimidal geometry[3] at the position corresponding to C1′. Unfortunately, a stable trigonal bipyrimidal isostere with functionality appropriate for the nucleoside hydrolase transition state is not available. Guided by the molecular electrostatic potential and the geometry of the transition state, additional aglycon derivatives of the phenyliminoribitol are being synthesized which are expected to simultaneously involve the proton-accepting interaction of N7 and maintain the hydrophobic effect enjoyed by phenyliminoribitol.

Transition-State Charge Mimicry. Every inhibitor which contains the iminoribitol ring binds substantially tighter than does inosine or any other known substrate for the enzyme (e.g., Table II). When acting as competitive inhibitors, the unsubstituted, imidazolyl-substituted, and phenyl-substituted iminoribitols bind 38, 127, and 2500 times more tightly, respectively, than inosine. Following slow-onset inhibition by phenyliminoribitol, the binding is approximately 12 500 tighter than inosine. These interactions represent energetic advantages of –2.2, –2.9, –4.7, and –5.7 kcal/mol, respectively. The value of –2.2 kcal/mol for the unsubstituted pyrrolidine is a lower limit for the energetic contribution of charge recognition. The nearest isostere to iminoribitol (**6**) is anhydroribitol (**4**) with the charge and hydrogens at the imino group being the sole differences. The binding of **6** is favored by –4.7 kcal/mol relative to **4**, suggestive of ion pair or strong hydrogen bond formation with iminoribitol. In the transition state, the charge is delocalized between the ribosyl residue and the departing aglycon functionality. The iminoribitol-based inhibitors concentrate the charge around the ammonium group, in contrast to the charge distribution found at the transition state (cf. Figures 2 and 3), reflecting the difference between fully formed covalent bonds and the partial bonds characteristic of the transition state.

The pH dependence of V_{max} and K_m for nucleoside hydrolase has established that two unprotonated enzymatic groups, both with pK_a values near 6.1, are required for catalysis, but substrate binding is independent of pH (Parkin et al., 1991a). This feature provides a convenient index for inhibitors acting as substrate or transition-state analogues. Substrate analogues which mimic the Michaelis complex are expected to bind in a pH-independent manner. Transition-state analogues are expected to be sensitive to ionization of the oxycarbonium mimic as well as the two enzymatic groups required for catalysis. In the case of the phenyliminoribitol (**8**), pK_a 6.5, optimal inhibition is expected at low pH values where the nitrogen is predominantly in the charged form, to mimic the oxycarbonium ion of the transition state. At higher pH values, the unprotonated phenyliminoribitol is expected to be less effective as an inhibitor if charge mimicry is the sole contribution to binding. The observation that the unprotonated inhibitors remain inhibitory at alkaline pH values requires that the inhibitors bind with an alternative favorable binding mode. The MEP of unprotonated phenyliminoribitol has little charge mimicry relative to the region corresponding to C1′–O4′ of the transition state. However, the NH hydrogen is available to function as a hydrogen bond donor and could interact strongly with an enzymic residue, such as an ionized carboxylate which normally functions to stabilize the oxycarbonium ion. Similar observations have been reported for other glycosidase inhibitors (Dale et al., 1985). The molecular basis for the approximately 100-fold lower basicity of **8** relative to **6** and **7** is uncertain. We speculate that a conformation-dependent H-bond between O5′–H and the pyrrolidine nitrogen or a perturbation of the nitrogen pK by the neighboring hydrophobic phenyl group may be responsible. The low pK_a values observed for the iminoribitol compounds could be explained by inductive effects of the hydroxyl groups. For comparison, pyrrolidine (C_4H_9N) has a pK_a of 11.

Imidazolyliminoribitol (**7**) has pK_a values at 5.2 (imidazole) and 8.7 (iminoribitol) but shows a similar effect of pH on the inhibition constants as does the phenyliminoribitol (**8**). The

[3] The assumption of trigonal bipyrimidal geometry results from model calculations on the hydrolysis of 2-(1-imidazolyl)tetrahydrofuran. The saddle point identified by ab initio calculations (STO-3G) was very nearly trigonal bipyrimidal. A similar result has been reported for the hydrolysis of nicotinamide riboside, using MOPAC calculations (Shröder et al., 1992).

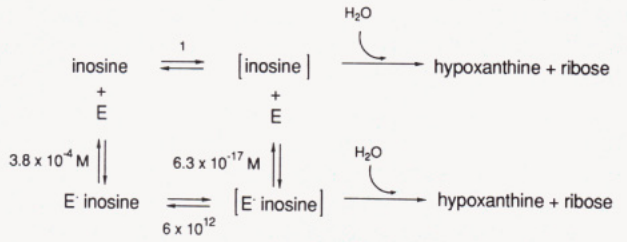

FIGURE 7: Thermodynamic box for transition-state stabilization by nucleoside hydrolase. The upper pathway represents the uncatalyzed hydrolysis of inosine at pH 7.0 and is assigned a value of 1. The rate acceleration for *N*-glycohydrolases similar to nucleoside hydrolase is estimated to be 6×10^{12} (see text). This value is attributed to transition-state stabilization in transition-state theory (bottom pathway). Enzymatic binding of inosine to form the Michaelis complex is shown on the left, while the binding of the transition state to the enzyme is shown on the right. The value of 6.3×10^{-17} M for binding the transition-state structure is from solution of the thermodynamic box. Transition-state structures are shown in brackets.

low pK_a of the imidazole nitrogen was not anticipated in the design of the compound. This feature renders the protonated N3 with its associated positive MEP inaccessible under normal assay conditions. Second-generation inhibitors with greater intrinsic basicity are being designed. Studies of the effects of pH on binding and catalysis of substrates and the iminoribitol inhibitors are currently underway to identify the ionic nature of the enzyme–inhibitor interactions. The results demonstrate that the protonated iminoribitols are bound tightly to nucleoside hydrolase, despite alternative binding modes. The binding of substituted iminoribitols depends on the ionization state of the oxycarbonium mimic and on enzymatic groups required for V_{max} (transition-state stabilization). These compounds therefore qualify as transition-state analogues.

Hydrophobic Effect. The nonpolar phenyl ring of phenyliminoribitol (**8**) increases the inhibition by a factor of 67 relative to iminoribitol (**6**), a difference in free energy of –2.5 kcal/mol. Following slow-onset inhibition, the presence of the phenyl group causes binding to be approximately 330-fold, or –3.5 kcal/mol more favorable. Substrate specificity studies (Table II) identified purine riboside as the tightest binding substrate at 145 μM. Purine riboside binds approximately three times tighter than either inosine (380 μM) or adenosine (460 μM). Purine riboside lacks a C6 substituent and is the most hydrophobic of the substrate aglycons. These results demonstrate that a portion of the aglycon binding pocket prefers interaction with hydrophobic residues. The larger dissociation constant observed for the most polar imidazole pyrrolidine is consistent with this hypothesis. Comparison of the MEP for the transition state and phenyliminoribitol (**8**) (Figure 2 and panel G of Figure 4) demonstrates the correlation between the hydrophobic interior of the hypoxanthine ring and the phenyl ring.

Many inhibitors which are mimics of transition-state structure exhibit an immediate as well as a time-delayed onset of inhibition [e.g., Morrison and Walsh (1988)]. Phenyliminoribitol (**8**) exhibits immediate competitive inhibition as well as a time-dependent onset of tight binding inhibition. No slow-onset binding was observed with the other iminoribitols. This may be due to the hydrophobic phenyl ring allowing access into a tighter, more transition-state-like binding mode [e.g., Merkler et al. (1990)]. One mechanism for slow-onset inhibition is a time-dependent conformational change of the enzyme to cause altered ribose pucker which gives alignment of the phenyl in the transition-state geometry. X-ray crystal structure will be needed to resolve this issue.

Theoretical Limits on Transition-State Mimicry. Nucleoside hydrolase, by analogy to AMP nucleosidase, a related

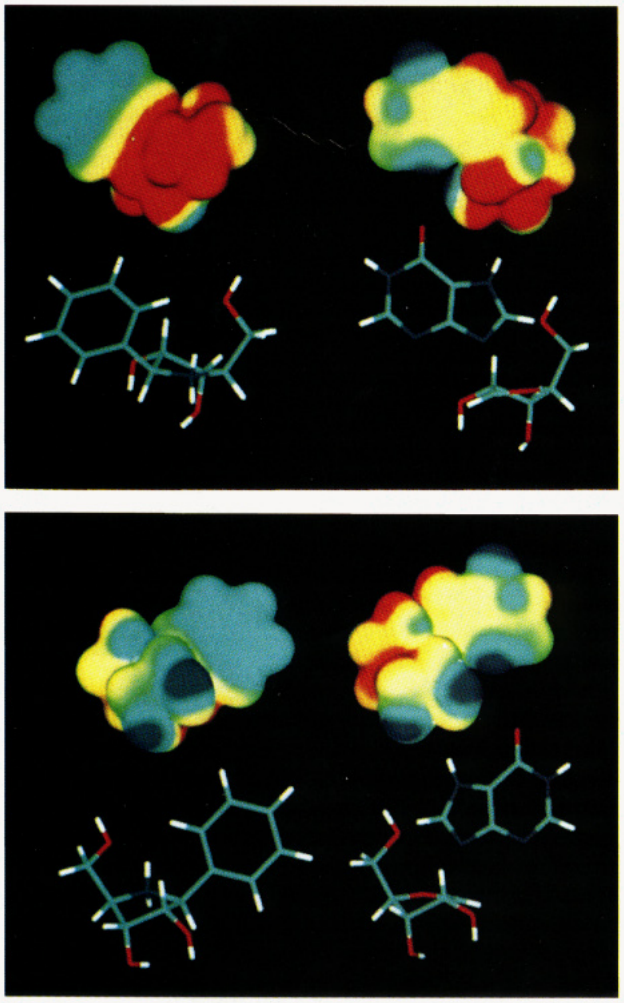

FIGURE 8: Comparison of the MEP surfaces for phenyliminoribitol and inosine at the transition state of nucleoside hydrolase. The left figures in the upper panel compare the stick and MEP surface for phenyliminoribitol. The view is looking toward the amino group of iminoribitol and the surface of the phenyl ring. The left figure in the lower panel is a 180° rotation of the figures above. The view is looking toward the 2′- and 3′-hydroxyls of the iminoribitol, thus blocking the view of the positive charge shown above. The right figure in the upper panel is the MEP surface for inosine at the transition state. The view is looking toward the oxycarbonium oxygen of ribose and the surface of the hypoxanthine ring. The right figure in the lower panel is a 180° rotation of the figures above. The view is looking toward the 2′- and 3′-hydroxyls of the ribose. Some of the oxycarbonium positive charge can be seen from this side. These views demonstrate that the positive charge on nitrogen of phenyliminoribitol is more localized than that on the oxycarbonium of the transition state.

N-glycohydrolase, accelerates hydrolysis of the N-glycosidic bond by a factor of 6×10^{12} relative to the uncatalyzed hydrolysis in water at neutral pH (Dewolf et al., 1979). This corresponds to a $\Delta G^{\ddagger}$ of –17.8 kcal/mol. Assuming that the entire catalytic acceleration results from transition-state stabilization, the theoretical binding constant for the transition state can be calculated. This value sets the upper limit for binding affinity of a transition-state analogue (Pauling, 1948; Wolfenden, 1969). As illustrated in Figure 7, a thermodynamic box can be used to describe interactions between inosine and its transition state and the binding of these species to nucleoside hydrolase. Using the K_d value of 380 μM for the interaction of the enzyme with inosine, and the rate acceleration of 6×10^{12}, a value of 6.3×10^{-17} M is calculated for the dissociation constant for $S^{\ddagger}$ from $ES^{\ddagger}$. The limiting inhibition constant observed in this study of approximately 3×10^{-8} M for the phenyliminoribitol (**8**) is approximately 11 kcal/mol

short of being a perfect transition-state analogue, utilizing only 5.7 kcal/mol of total binding energy toward transition-state recognition. This shortfall is due to geometric factors and the imperfect match of charge between phenyliminoribitol and the transition state (Figure 8). Although both sides of the inhibitor are similar in charge distribution to the transition state, an exact match is not possible. Fortunately, only a similarity to the transition-state structure is required to capture sufficient binding energy to yield a physiologically effective inhibitor.

For nucleoside hydrolase, the carbon–carbon glycosidic bond prevents the electronic distribution from matching that of the transition state but provides a structure stable to enzymatic or chemical solvolysis. The sp^3 hybridization at C1′ of the inhibitors causes a geometric anomaly compared to the actual transition state, again altering the match from perfect transition-state contacts. Nonetheless, the estimated 30 nM dissociation constant for the phenyliminoribitol makes it a powerful inhibitor of nucleoside hydrolase. With an inhibition constant of 30 nM, a $10K_i$ level of inhibition could be provided to 30 L of solution using less than 2 mg of the inhibitor.

Use of Molecular Electrostatic Potential for Inhibitor Design. Comparison between the MEP of the transition state and of candidate inhibitors forms the basis for use of MEP in inhibitor design. Current interpretation of the MEP calculations is by a qualitative analysis. Thus, regions of the transition-state structure having a highly positive electrostatic potential are those most likely to interact with electron-rich enzymatic residues, when the enzyme is in its transition-state-stabilizing configuration. An inhibitor with a similar MEP is presumed to undergo a similar interaction with the transition-state configuration of the enzyme and is visualized in a conformation similar to that of the deduced transition state. Analytical calculations that estimate the energetics of transition-state correlation for a family of potential inhibitors have not yet been implemented. A procedure which describes a method for the alignment of molecular structures by maximizing electrostatic potential and steric overlaps has been described (Smith, 1988), but this has not yet been applied to transition states. Development of such algorithms is in progress and may permit a quantitative correlation of inhibitors with the transition state.

The sequential application of experimentally measured kinetic isotope effects, bond vibrational analysis, and molecular electrostatic potential provides sufficient transition-state information to permit the rapid design of transition-state inhibitors. This method differs fundamentally from X-ray crystallographic or other spectroscopic techniques which characterize ground states. However, the full potential of transition-state analysis will be reached when inhibitors designed to mimic known transition states can be characterized by crystallographic methods [e.g., Lolis and Petsko (1990)]. Until then, the utility of transition-state analysis will clearly be to provide a rapid route to the design and synthesis of inhibitors for any enzyme whose transition state can be solved by families of kinetic isotope effects [e.g., Mentch et al. (1987), Markham et al. (1987), Parkin et al. (1991b), and Horenstein et al. (1991)].

ACKNOWLEDGMENT

The authors thank Dr. Khalil Abboud, Department of Chemistry, University of Florida, Gainesville, FL, for solving the crystal structure of anhydroribitol.

REFERENCES

Angelotti, T., Krisko, M., O'Connor, T., & Serianni, A. S. (1987) *J. Am. Chem. Soc. 109*, 4464–4472.
Bennek, J. A., & Gray, G. R. (1987) *J. Org. Chem. 52*, 892–897.
Cleland, W. W. (1977) *Adv. Enzymol. Relat. Areas Mol. Biol. 45*, 273–387.
Dale, M. P., Ensley, H. E., Kern, K., Sastry, K. A. R., & Byers, L. D. (1985) *Biochemistry 24*, 3530–3539.
DeWolf, W. E., Jr., Fullin, F. A., & Schramm, V. L. (1979) *J. Biol. Chem. 254*, 10868–10875.
Endo, A., Kuroda, M., & Tanzawa, K. (1976) *FEBS Lett. 72*, 323–326.
Fleet, G. W. J., & Son, J. C. (1988) *Tetrahedron 44*, 2637–2647.
Frisch, M. J., Trucks, G. W., Head-Gordon, M., Gill, P. M. W., Wong, M. W., Foresman, J. B., Johnson, B. G., Schlegel, H. B., Robb, M. A., Replogle, E. S., Gomperts, R., Andres, J. L., Raghavachari, K., Binkley, J. S., Gonzalez, C., Martin, R. L., Fox, D. J., DeFrees, D. J., Baker, J., Stewart, J. J. P., & Pople, J. A. (1992) *Gaussian 92, Revision A*, Gaussian, Inc., Pittsburgh, PA.
Horenstein, B. A., & Schramm, V. L. (1993) *Biochemistry 32*, 7089–7097.
Horenstein, B. A., Parkin, D. W., Estupinan, B., & Schramm, V. L. (1991) *Biochemistry 30*, 10788–10795.
Kinoshita, Y., Ruble, J. R., & Jeffrey, G. A. (1981) *Carbohydr. Res. 92*, 1–7.
Lienhard, G. E. (1973) *Science 180*, 149–154.
Lolis, E., & Petsko, G. A. (1990) *Annu. Rev. Biochem. 59*, 597–630.
Markham, G. D., Parkin, D. W., Mentch, F., & Schramm, V. L. (1987) *J. Biol. Chem. 262*, 5609–5615.
Mentch, F., Parkin, D. W., & Schramm, V. L. (1987) *Biochemistry 26*, 921–930.
Merkler, D. J., Brenowitz, M., & Schramm, V. L. (1990) *Biochemistry 29*, 8358–8364.
Morrison, J. F., & Walsh, C. T. (1988) *Adv. Enzymol. Relat. Areas Mol. Biol. 61*, 201–301.
Munns, A. R. I., & Tollin, P. (1970) *Acta Crystallogr., Sect. B 26*, 1101.
Niwa, T., Inouye, S., Tsuruoka, T., Koaze, Y., & Niida, T. (1970) *Agric. Biol. Chem. 34*, 966–988.
Parkin, D. W., Horenstein, B. A., Abdulah, D. R., Estupinan, B., & Schramm, V. L. (1991a) *J. Biol. Chem. 266*, 20658–20665.
Parkin, D. W., Mentch, F., Banks, G. A., Horenstein, B. A., & Schramm, V. L. (1991b) *Biochemistry 30*, 4586–4594.
Pauling, L. (1948) *Am. Sci. 36*, 50–58.
Sawa, T., Fukagawa, Y., Homma, I., Takeuchi, T., & Umezawa, H. (1967) *J. Antibiot. 201*, 227–231.
Shröder, S., Buckely, N., Oppenheimer, N. J., & Kollman, P. A. (1992) *J. Am. Chem. Soc. 114*, 8232–8238.
Sims, L. B., & Lewis, D. E. (1984) in *Isotopes in Organic Chemistry* (Buncel, E., & Lee, C. C., Eds.) p 161, Elsevier, New York.
Sims, L. B., Burton, G. W., & Lewis, D. E. (1977) *Quantum Chemistry Program Exchange*, No. 337, Indiana University, Bloomington, IN.
Smith, G. M. (1988) *Quantum Chemistry Program Exchange*, No. 567, Indiana University, Bloomington, IN.
Thomson, C. (1989) in *Quantitative Structure–Activity Relationships in Drug Design*, pp 269–274, Alan R. Liss, Inc., New York.
Umezawa, H., Aoyagi, T., Morishimia, H., Matzusaki, M., Hamada, H., & Takeuchi, T. (1970) *J. Antibiot. 23*, 259–262.
Weiner, P. K., Langridge, R., Blaney, J. M., Schaefer, R., & Kollman, P. A. (1982) *Proc. Natl. Acad. Sci. U.S.A. 79*, 3754–3758.
Wolfenden, R. (1969) *Nature (London) 223*, 704–705.
Wolfenden, R. (1972) *Acc. Chem. Res. 5*, 10–18.
Wolfenden, R., & Kati, W. M. (1991) *Acc. Chem. Res. 24*, 209–215.